IET Generation, Transmission & Distribution

Special Issue: Optimal Utilisation of Storage Systems in Transmission and Distribution Systems

Application of a battery energy storage for frequency regulation and peak shaving in a wind diesel power system

ISSN 1751-8687
Received on 31st March 2015
Revised on 31st July 2015
Accepted on 11th August 2015
doi: 10.1049/iet-gtd.2015.0435
www.ietdl.org

Rafael Sebastián ✉

Department of Electrical, Electronic and Control Engineering (DIEEC), Spanish University for Distance Education (UNED), Madrid 28040, Spain
✉ *E-mail: rsebastian@ieec.uned.es*

Abstract: This study presents the modelling and dynamic simulation of a high penetration wind diesel power system (WDPS) consisting of a diesel generator (DG), a wind turbine generator (WTG), consumer load, dump load and a battery energy storage system (BESS). First the WDPS architecture and the models of the WDPS components are described. The WDPS is simulated in wind-only (WO) mode where the DG is not running and the WTG supply active power and in wind-diesel (WD) mode where both DG and WTG supply power. The simulation results are given showing graphs of the main electric variables in the WDPS (system frequency and voltage and active power in each component) and main battery variables (current, voltage and state of charge). The results in the WO mode show how the BESS, under the command of a proportional-integral-derivative (PID) controller, supplies/stores active power to regulate the isolated system frequency. The WD control enables the BESS to smooth the load and wind power variations, so that the isolated system power quality is improved. Also it is shown in the WD mode a peak shaving application where the control orders the BESS to supply active power temporarily to support system frequency in a DG overload situation.

1 Introduction

Wind diesel power systems (WDPSs) are isolated power systems combining wind turbine generators (WTGs) with diesel generators (DGs) to obtain the maximum contribution by the intermittent wind resource. This is in order to reduce the fuel consumption and so lowering the running costs and environmental impact. WDPSs have three operation modes [1]: diesel-only (DO), wind-diesel (WD) and wind-only (WO). In the DO mode, the DGs supply the active and reactive power, the WTGs are disconnected and the WDPS works as a conventional diesel power plant. Load sharing and speed regulators controlling each diesel engine (DE) perform frequency regulation and voltage regulation is performed by the synchronous voltage regulators in each generator. In the WD mode, both the WTGs and the DGs supply power. The same regulators as in the DO mode are in charge of the control of the frequency and the voltage. In the WO mode, the DGs are not running, the wind turbines (WTs) are supplying active power and therefore, auxiliary components are needed to control frequency and voltage in the isolated power system. This third mode is only available in high wind penetration WDPS (HP-WDPS).

In the WD mode the net load, defined as the consumer load minus the WTGs produced power, is reduced but the corresponding fuel saving is not as high as expected. This is because an unloaded DG can consume fuel up to 40% of nominal fuel consumption [2]. In addition, the intermittent nature of the wind makes the WTGs produced power very unpredictable, so that the number of DGs needed to supply the instantaneous net load plus the required spinning reserve change very often. This leads to an excessive number of starts/stops in the DGs and the additional DGs wearing and fuel consumption. In order to effectively reduce the fuel consumption and the number of the DGs start–stop cycles, the WDPS can incorporate a short-term energy storage system (ESS) [3]. The short-term ESS is used to cover peaks in the net load due to stochastic wind and load variations and to store temporally the wind power excess during the periods of strong wind and/or low consumer load. The addition of a short-term ESS covering the average load for just minutes will significantly reduce the number of start–stop cycles in the DGs, with acceptable levels with just a minute [2].

Several studies demonstrate that ESSs improve the power quality of the power produced by WTGs connected to large power systems. In [4, 5], the ESS is based on flywheels (FESS-flywheel ESS) and in [6, 7] is based on batteries (BESS-battery ESS). WDPSs are isolated low inertia power systems where significant frequency and voltage deviations occur, so the power quality improvement obtained by adding an ESS is more effective in this case. Examples of ESSs in WDPS are [8] with BESS, [9] with FESS and [10] with capacitive ESS.

Several papers have been published on the subject of WDPS dynamic simulation. In [11], a no-storage WDPS is simulated in several cases, among them the connection of a WTG to the DG isolated grid (DO-to-WD mode transitions). In [12], a no storage WDPS consisting of three WTGs and two DGs is simulated against several perturbations, among them sudden changes in load demand and sudden disconnection of the WTGs. The previous article [8] deals with a medium penetration WDPS (no WO mode) with a BESS and shows how the WDPS control uses the BESS as an artificial load to avoid a reverse power situation in the DG. In previous article [13], the HP-WDPS includes a BESS and it is simulated a WO-to-WD mode transition in order to substitute a supplying BESS by the DG.

After this introductory Section 1, this paper is organised as follows: Section 2 presents the WDPS architecture discussed in this paper and the modelling of the WDPS components, Section 3 presents the WO mode control to regulate system frequency along with the WO simulations, Section 4 presents the WD mode control and the WD simulations which include a peak-shaving application, and finally Section 5 summarises the benefits of using the BESS and its associated controls in the WDPS.

2 Isolated WDPS modelling

The HP-WDPS discussed in this paper is presented in Fig. 1. The DG includes a friction clutch, which has three states: engaged,

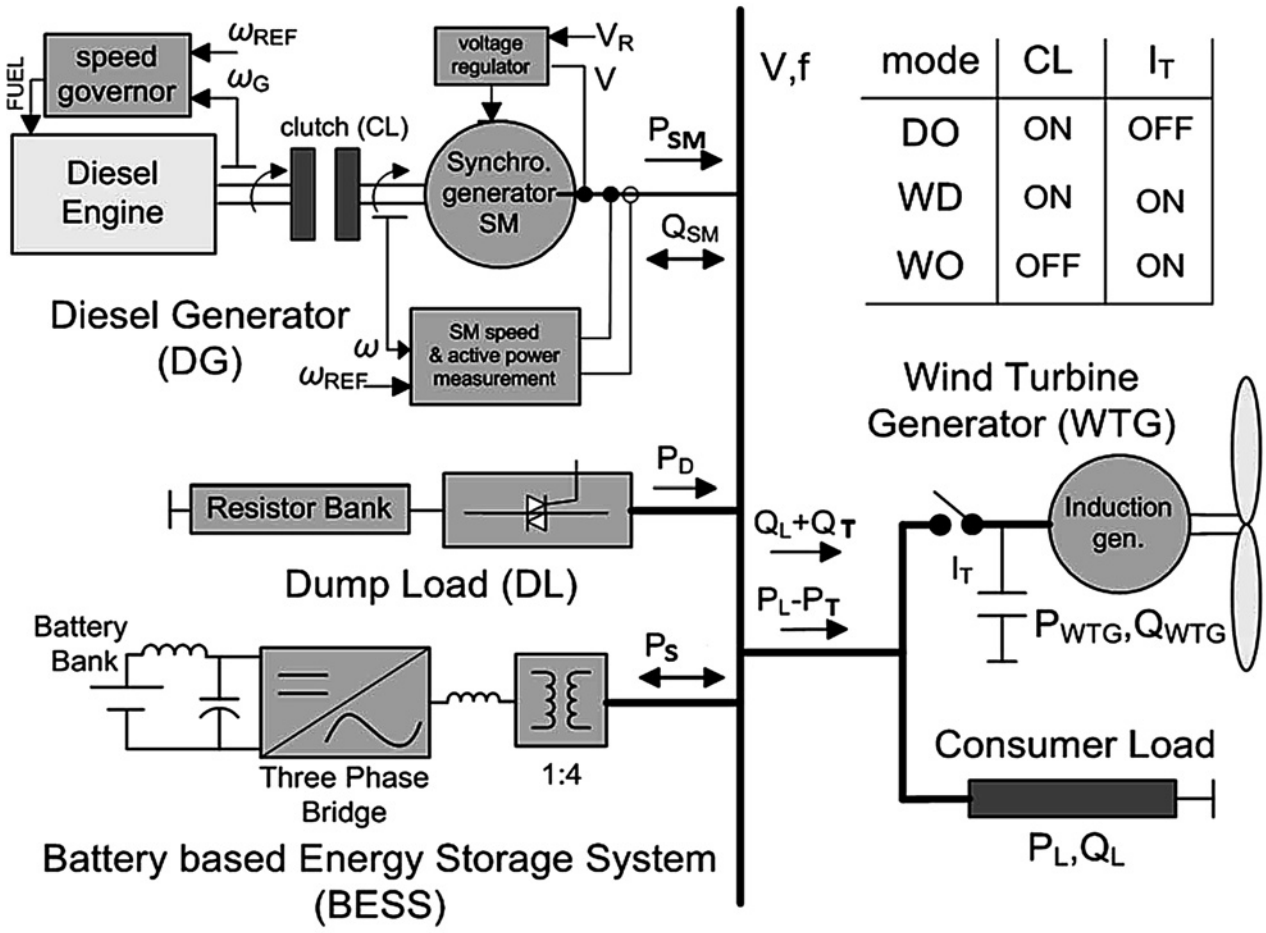

Fig. 1 *Layout of the HP-WDPS with BESS*

locked and disengaged [14]. If the clutch is disengaged (OFF in Fig. 1), then the clutch surfaces are not in contact and the DE does not transfer any torque to the synchronous machine (SM), so that if the WTG circuit breaker I_T is closed, the operation mode is WO. In the clutch engaged state, the frictional surfaces slip past one another and kinetic friction torque is transferred to the SM. With the clutch locked (ON in Fig. 1), the frictional surfaces are locked together without slipping and DE and SM shafts behave as one shaft ($\omega_g = \omega$ in Fig. 1). In the clutch-locked state, the DE transfers torque to the SM and the WDPS is in the DO/WD mode if the WTG circuit breaker I_T is opened/closed respectively.

The WDPS of Fig. 1 has been simulated using MATLAB-Simulink simulation software. In the following subsections, the models of the WDPS components are described.

2.1 DG model

The DG of Fig. 1 comprises a DE, a SM and a clutch. With the clutch locked the set DE + SM behaves as a DG set.

The DE isochronous speed governor commands the necessary fuel rate to make the DG run at constant speed (isochronous speed control) ω_g and therefore, constant system frequency f. The models of the DE and its speed regulator and actuator follow the ones presented in [15]. The DE model has the current DE speed ω_g (pu) as input, and outputs the mechanical power P_{DE} (pu) to take the DE speed to 1 pu speed reference ω_{ref}. The DE has been simulated by means of a gain, relating fuelling rate to torque, and a dead time, modelling the firing delay between pistons. The actuator has been modelled as a second-order system and the speed regulator is a PID control.

The SM provides the voltage waveform of WDPS in the three modes considered, so it must be always connected to the isolated grid and SM speed must be close to rated. The SM automatic voltage regulator (AVR) controls the voltage module to be within the prescribed levels. The SM has a rated power of 300 kVA and its model comes from the SymPower System blockset [16]. The SM electrical part is represented by a sixth-order model and its voltage regulator–exciter is an IEEE type 1 model. The inertia constant H range in synchronous condensers spans from 1 to 1.5 s, [17] and 1 s is assigned to SM inertia constant (H_{SM}) as it is a low-power one. The inertia constant for the set SM + DE (DG, clutch locked) H_{DG} is 1.75 s.

2.2 WTG model

The WTG in Fig. 1 consists of a WT driving an induction generator (IG) of 275 kW (WTG rated power $P_{T\text{-}NOM} = 275$ kW) directly connected to the isolated grid conforming a constant speed stall-controlled WTG (no pitch control). This kind of WTGs has no means to control the produced active power (P_T), which depends among other factors on the cube of the wind speed, but it has robust construction, low cost and simply maintenance and these are important factors in the remote locations of WDPS. The IG consumes reactive power so a capacitor bank has been added in Fig. 1 to compensate the power factor. The IG model comes from SymPower System blockset [16] and its electrical part is represented by a fourth-order model. The no pitch control WT model follows the one in [18] and it is simulated using the WT characteristics. The WT characteristics output the mechanical power in the WT shaft $P_{T\text{-}MEC}$ as a function of the wind speed and the WT shaft speed (ω_WT). As Fig. 2 shows $P_{T\text{-}MEC}$ is divided

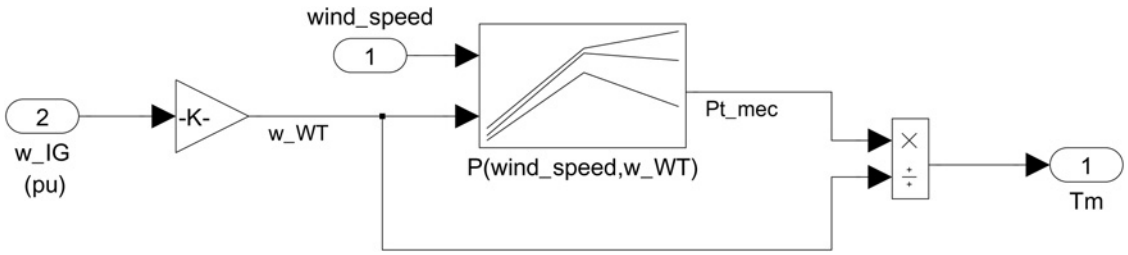

Fig. 2 *WT-Simulink schematic*

by the WT speed to calculate the torque *Tm* applied to the WTG-IG. Typical inertia constant H_W values for WTGs are between 2 and 6 s [19]. As the WTG used in the paper is a low-power one, the low limit of the previous range, 2 s, is assigned to H_W.

2.3 Dump load (DL) model

The DL of Fig. 1 consists of eight three-phase resistors, each one connected in series with three semiconductor power switches (one switch per phase). By closing/opening one set of three switches, the corresponding three-phase resistor is connected/disconnected from the isolated grid, so the active power absorbed by the DL can be controlled to create a controlled sink of active power. In a real implementation, the power switches are Gate Turn OFF (GTO) semiconductor switches. The resistor values follow an 8-bit binary progression, so that the power consumed by the DL, assuming that the voltage in the isolated grid is nominal, can be expressed in the form

$$(I_0 + I_1 \cdot 2^1 + \cdots + I_7 \cdot 2^7) \cdot P_{\text{STEP}} = X_{\text{D-REF}} \cdot P_{\text{STEP}} \quad (1)$$

where P_{STEP} is the power corresponding to the least significant bit I_0 and therefore the highest value three-phase resistor, I_j is '1' when the associated GTO is turned on, so its associated three-phase resistor is connected to the isolated grid, and '0' when the GTO is turned off. According to (1), the DL-consumed power can be varied discretely from 0 (all the GTOs OFF) to $255 \cdot P_{\text{STEP}}$ (all the GTOs ON). In this paper, $P_{\text{STEP}} = 1.4$ kW and therefore $P_{\text{D-NOM}} = 357$ kW (which is a 30% greater than $P_{\text{T-NOM}}$). The DL is used in the WD mode to load artificially the isolated power system when the WTG-produced power is greater than the load consumed power, so that the needed DG active power is positive and the DG reverse power situation is avoided [8]. In the WO mode, the DL is used to consume the wind power excess in order to regulate system frequency [20].

2.4 BESS model

The BESS of Fig. 1 is based on a 240 V Ni–Cd battery bank, a LC filter, an IGBT three-phase bidirectional current controlled inverter (CCI) of rated power $P_{\text{S-MOM}} = 150$ kW and a 150 kVA elevating transformer.

The CCI performs the DC/AC conversion to interface the battery bank to the isolated grid. The CCI can operate as an inverter by supplying power to the isolated grid (discharging the battery) or as a rectifier by absorbing power from the isolated grid (charging the battery). In order to reduce the converter sizing its reactive power reference is null, so it works with 1 power factor. The grid converter uses IGBTs and the harmonic current injection to the isolated grid is limited by means of an L-filter. A detailed description of this converter can be seen in [21].

The elevating transformer (120/480 VAC) isolates the three-phase bridge and the battery bank from the isolated grid and allows using a 240 V standard battery voltage. Other arrangements to connect the battery to the grid are possible. For example, the BESS in [22] has no transformer, so the inverter is connected directly to the isolated grid and to elevate the battery voltage up to the needed inverter DC input voltage a bi-directional DC/DC buck–boost converter is used.

The model for the 240 V Ni–Cd battery [23] comprises a variable DC voltage source in series with an internal constant resistance. The voltage source value depends on the battery state of charge (SOC) according to the battery discharge curve and the internal resistance has the same constant value for charging and discharging. Other battery models can be seen in [7, 24]. The energy stored in the battery is 93.75 kWh for producing the converter rated power 150 kW during 15 min and with operating range between 35 and 75% of its rated capacity, so its stored energy is 150 kW·15 min/(0.4·60 min/h) = 93.75 kWh [25]. In a Ni–Cd battery string of voltage 240 V, this corresponds to a capacity C of 390.625 Ah (93.75 kWh/240 V = 390.625 Ah). Finally, an LC filter limits the battery current ripple.

The BESS can also be used with the same aim as the DL, i.e. as an artificial load in the WDPS to avoid the reverse power in the DG [8]. Additionally the BESS can reduce in both DO and WD modes the needs of spinning reserve, increase the loading to the DGs in order to improve their performance and improve the power quality of the WDPS. In the WO mode, the BESS is used to consume the wind power excess or supply the active power deficit to balance active power in order to regulate system frequency.

3 WO mode

In the WO mode, the WTG is the only power source, so this mode is only possible if most of the time the power coming from the WTG is greater than the consumed power by the load. In the WO mode, the clutch is disengaged, so that the DE and SM shafts are independent, the SM input torque is zero and the SM behaves as a synchronous condenser providing the voltage waveform to the isolated grid.

The system frequency is regulated by maintaining an instantaneous balance of the active power consumed and produced. The active power consumed by the load (P_L) is produced only by the WTG (P_T). Since P_T (also called wind power) and P_L are uncontrolled, the DL + BESS must perform the instantaneous balance of the active power. To accomplish this active power balance, the BESS can store the surplus active power from the WTG ($P_T > P_L$) or supply power ($P_T < P_L$) in the periods when the wind power is less than current load; also the surplus wind power can be consumed by DL. With P_D the power consumed by the DL, P_S the power consumed/supplied by the BESS, J_{SM} the SM inertia and ω the SM shaft speed, the power equation of the SM in WO mode if no losses are taking into account is

$$P_T - P_L - P_D - P_S = J_{SM}\omega\frac{d\omega}{dt} \quad (2)$$

where P_T is considered positive if produced and P_L, P_D and P_S are considered positive if consumed. In (2), the SM shaft speed ω is in rad/s and it is related with the system frequency (frequency of the voltage waveform) f by $\omega = 2\pi f/p$, with p the number of pole pairs of SM. To obtain a synchronous shaft speed (system frequency) constant ($d\omega/dt = 0$), the DL + BESS combination must consume power when P_T exceeds P_L and the BESS must generate power when P_T is less than P_L.

IET Gener. Transm. Distrib., 2016, Vol. 10, Iss. 3, pp. 764–770

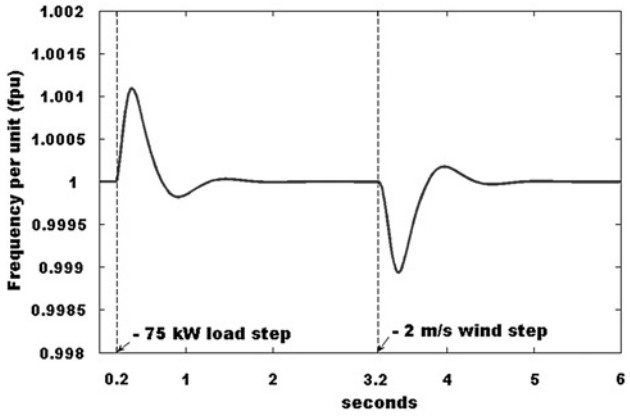

Fig. 3 *WO mode frequency per unit*

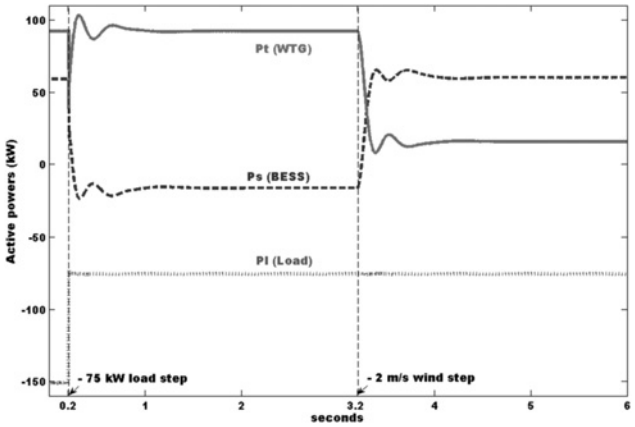

Fig. 5 *WO mode active powers by the WTG, BESS and load*

The reference power P_{REF} needed to be absorbed ($P_{REF} > 0$) by the DL + BESS combination or to be supplied ($P_{REF} < 0$) by the BESS to control the isolated power system frequency is calculated in the WO mode by a PID regulator, whose input is the system frequency error e_f ($e_f = f - f_{NOM}$, where f_{NOM} is the power system nominal frequency and f the current system frequency) and whose output is P_{REF} [26]. The integral part of the PID eliminates the steady-state frequency error, performing an isochronous speed control. The system frequency is obtained by measuring the SM shaft speed ω as Fig. 1 shows.

The power sharing between DL and BESS when $P_{REF} > 0$ is calculated by means of

$$P_{REF} = P_{S-REF} + P_{D-REF} \tag{3}$$

$$P_{D-REF} = 0, \text{ if } P_{REF} < P_{S-NOM} \tag{4}$$

where $P_{D\text{-}REF}$ is the reference power to be dumped by DL and $P_{S\text{-}REF}$ the reference power to be stored/retrieved by BESS. Equation (4) means that the DL does not actuate unless the P_{REF} needed is greater than the BESS rated power $P_{S\text{-}NOM}$, guaranteeing that the DL will only dump just the excess wind power that the BESS cannot store [13].

The WDPS of Fig. 1 was simulated in the WO mode and the simulations include a negative consumer load step of 75 kW at t = 0.2 s and a negative wind speed step of 2 m/s at t = 3.2 s. In a real system, the variations will be more progressive and these sudden changes are considered the worst cases. The fast dynamics of the BESS power converter is able to follow the reference power P_{REF} from the PID regulator almost instantly. The simulation results are presented with graphs for the system frequency and the root mean square (RMS) voltage in the pu value in Figs. 3 and 4 respectively, the active powers (kW) for the WTG, consumer load and BESS in Fig. 5 and the battery variables in Fig. 6. The active powers are considered positive/negative when are produced/consumed, so that the sum of active powers in Fig. 5 is null whenever the power system is in equilibrium. At the starting point in t = 0 s, the active power consumed by the load is −150 kW. The wind speed is 8 m/s and the active power produced by the WTG is 92 kW. The BESS is supplying the active power deficit 58 kW. The isolated power system is in the steady state. The active power consumed by the DL is not shown in Fig. 5 as the DL is not needed ($P_{REF} < P_{S\text{-}NOM}$) throughout the tests presented in this simulation.

3.1 Negative load step

Starting at the described initial state, a negative step of 75 kW in the consumer load is applied at t = 0.2 s, so that the remaining load (75 kW) is lower than the WTG produced power. Fig. 5 shows the negative load step, how the BESS active power changes from 58 kW (producing) to −17 kW (consuming) and a transient in the WTG active power due to the load disconnection. During the transient due to the negative load step the frequency increases due to the active power surplus, being its maximum 1.0011 pu (Fig. 3) and the RMS voltage presents a maximum of 1.062 pu. In the steady state reached at t = 1.721 s, the WTG produced active power stays at the same initial value (92 kW) as the wind speed has not changed and the BESS consumes the WTG active power excess.

3.2 Negative wind step

In t = 3.2 s. the wind speed changes from 8 to 6 m/s. Fig. 5 shows that the power produced by the WTG decreases and reaches

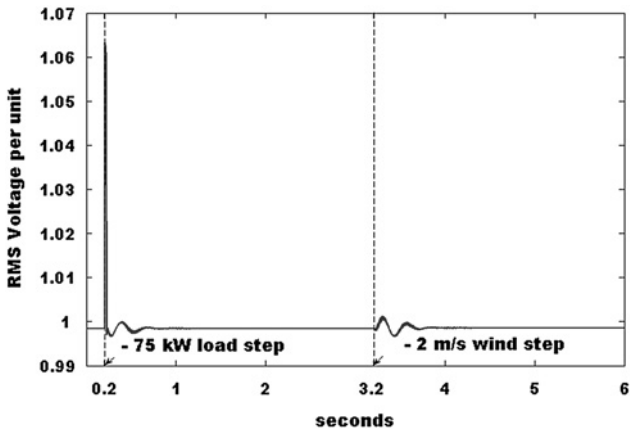

Fig. 4 *WO mode RMS voltage per unit*

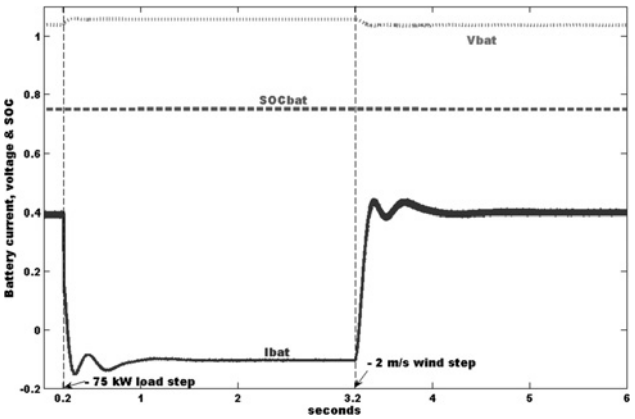

Fig. 6 *WO mode battery current, voltage and SOC*

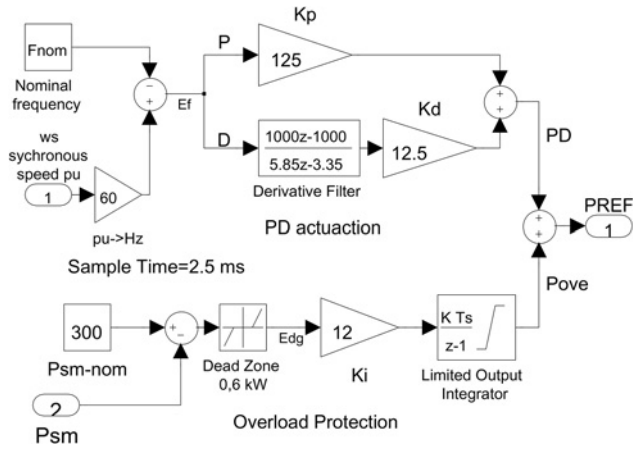

Fig. 7 *WD mode control schematic*

16 kW in the steady state. During the transient due to the negative wind step change, the frequency decreases due to the active power deficit being its minimum 0.9987 pu. In $t = 4.805$ s the transient finishes with the BESS supplying the active power deficit of 59 kW.

The battery voltage (normalised to its rated voltage 240 V), the battery current (normalised to its rated current 150 kW/240 V = 625 A), and the SOC (in pu) are shown in Fig. 6. The battery current is considered positive when discharging and negative when charging. Fig. 6 shows that the battery current is approximately a scaled version of the BESS active power in Fig. 5. This is because the battery voltage is almost a constant value during the simulation ($P_S = I_{BAT} \cdot V_{BAT}$ by neglecting losses). The SOC, initially at 75%, scarcely changes due to the short simulation time and the relatively large battery capacity. The variations of the battery voltage are small and follow the current variations due to the internal battery resistance since the SOC variations are negligible.

The WO mode simulations have shown how the BESS under the command of a PID regulator balances the WDPS active power in order to regulate system frequency. In the presented simulation, the BESS changes from producing the active power deficit to consuming the active power excess and vice versa. In the final state, the BESS is supplying power and since the BESS stored power is limited, if the situation persists the control must order to start the DE and lock the clutch when DE speed reaches the rated speed, in order to substitute the supplying BESS with the DE, performing a controlled WO-to-WD mode transition [13].

Finally to remark that in both the initial and final states the BESS is supplying power so these states cannot be reached in a WDPS with no storage since the DL can only consume power, so the WO presented simulations can only be performed in a WDPS with an ESS.

4 WD mode

In the WD mode, the clutch is locked and the DE and SM behave as a DG set. The speed control of the DE of Fig. 1 is isochronous so the DG will run at constant speed provided that the demanded load is in the range spanning from 0 to its rated power. The diesel speed governor controlling the DE performs the frequency regulation by maintaining an instantaneous balance between the consumed and produced active power. To obtain the power equation of the SM in WD mode the mechanical power supplied by the DE, P_{DE} (positive when produced) must be added to (2) and J_{SM} must be substituted by the DG inertia J_{DG}

$$P_{DE} + P_T - P_L - P_D - P_S = J_{DG}\omega\frac{d\omega}{dt} \tag{5}$$

The diesel speed governor will make the DG run at constant speed ($d\omega/dt = 0$) by setting P_{DE}, so that the generated power is equal to the net consumed power P_L–P_T. However, the diesel speed governor cannot control P_{DE} (and therefore the frequency regulation is lost) if the needed P_{DE} is out of the range 0- DE rated power. The zero lower limit cannot be assured if the power supplied by the WTG surpass that consumed by the load (P_L–$P_T < 0$) because a negative power in the DG is needed to balance active powers (DG reverse power) and the diesel speed governor cannot order DE to consume power. A modern variable speed WTG, which can control the active power produced, can be used to prevent the reverse power situation by reducing P_T. However with the fixed speed no pitch control WTG used in this paper, to prevent the reverse power, the WDPS control system must order the DL, BESS or both to consume active power in order to need a positive P_{DE} to balance active powers in (5). With $P_{DE} > 0$, the speed governor will resume the control of the system frequency [8].

The net consumed power can be greater than the DG rated power and in this situation another DG must be connected to the isolated system in order to increase the isolated power system available rated power. However, time is needed for a new DG to start, get the nominal speed, synchronise with the grid voltage and connect the circuit breaker. In the simulations ahead it is shown in a DG overload situation how the control orders the BESS to supply active power temporarily to the system to sustain system frequency while waiting the new incoming DG. In a no-storage WDPS the previous DG overload situation can lead to a blackout, so to prevent this, spinning reserve must be provided and the DGs work partially loaded and therefore with low performance. The needs of spinning reserve are reduced in the WDPS of Fig. 1 in the rated power of the BESS $P_{S\text{-}NOM}$, because any time it is needed, the BESS can supply up to its nominal active power to the isolated grid.

In the WD mode, the needed reference power P_{REF} to be absorbed ($P_{REF} > 0$) by the DL + BESS combination or to be supplied ($P_{REF} < 0$) by the BESS for balancing the active power in the system is calculated by the sum of a proportional plus derivative control (PD) applied to the frequency error e_f and the term P_{MXN} which depends on the current active power supplied by the DG and prevents the DE from the reverse power situation when the electrical power generated by the SM P_{SM} is below a minimum [8] ($P_{SM} < P_{MIN}$) or from being overloaded when P_{SM} is over a maximum ($P_{SM} > P_{MAX}$)

$$P_{REF} = K_P e_f + K_D\frac{de_f}{dt} + P_{MXN} \tag{6}$$

The schematic of (6) (positive when consumed, negative when produced) is shown in Fig. 7 with the form of P_{MXN} for the overload situation. The form of P_{MXN} for the reverse power situation can be seen in [8]. The proportional and derivative constants K_P and K_D respectively (values in Fig. 7), has been chosen to position the dominant pole pair of the WDPS linearised model to be a double pole in order to increase the speed of response, reducing the settling time and minimising the system frequency over/under shooting [21]. This PD control is compatible with the DE PID isochronous speed controller which has the integral actuation to correct the steady-state frequency error. The DG overload protection control is a simple integral control with the P_{SM} as input, the 300 kW $P_{DG\text{-}MAX}$ maximum SM power as reference ($P_{SM\text{-}NOM}$) and the power to be produced by the BESS as output (P_{OVE}). The 0–6 kW dead zone (2% of $P_{SM\text{-}NOM}$) implements an offset to avoid excessive action of this protective control. When this protection is activated steady-state DG power is kept in the range from 294 to 300 kW. The system frequency f and SM active power P_{SM} variables needed for the described WD control are provided by Fig. 1 measurement block which measures the SM shaft speed ω to obtain f and the SM voltages and currents to obtain P_{SM}.

Simulation results in the WD mode are shown in Figs. 8–10 considering the variables: frequency per unit (fpu) (Fig. 8), RMS voltage per unit (Fig. 9) and active powers (positive when generated) for the WTG, DG, BESS and consumer load (Fig. 10) in kW. The active power consumed by the DL is not shown in

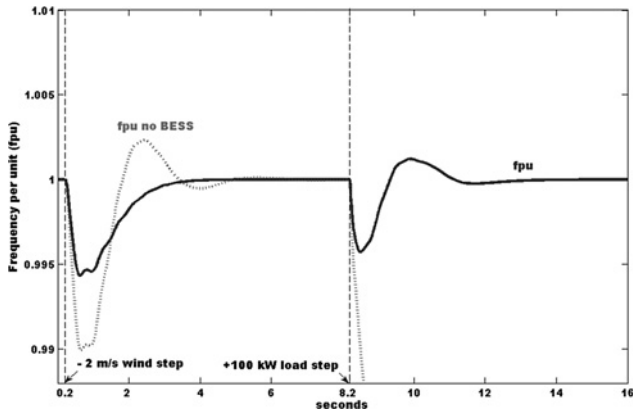

Fig. 8 *WD mode frequency per unit in the BESS/no BESS case*

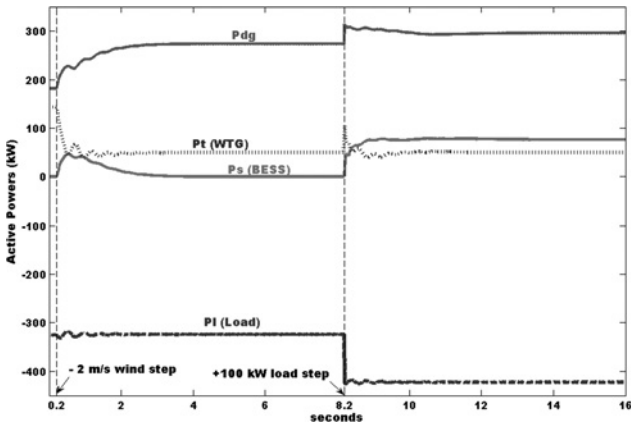

Fig. 10 *WD mode active powers by the DG, WTG, BESS and load*

Fig. 10 as the DL is not needed ($P_{REF} < P_{S\text{-}NOM}$) throughout the tests presented in this simulation. At the test starting point the wind speed is 9 m/s, the WTG and DG are producing active powers of 144 and 181 kW respectively, the load and BESS are consuming active powers of 325 and 0 kW respectively and the battery SOC is 75%, being the system at the steady state.

4.1 Negative wind step

In $t = 0.2$ s, the wind speed changes suddenly from its initial value of 9 to 7 m/s. Fig. 10 shows the corresponding decreasing in the WTG power from its initial 144 to 50 kW in the steady state. The WTG power decreasing leads to an active power deficit and a fall in the system frequency with fpu minimum of 0.9944. The minimum/maximum voltages during this negative wind step are 0.9811/1.0066 pu. Fig. 10 shows that the DG power is monotonically increasing and also that the BESS produces active power throughout the transient to compensate the active power deficit. In the steady state, reached at $t = 4.52$ s, the BESS power is null and the DG accommodates its output power to the new situation generating 275 kW. To remark the dynamic benefits of using the BESS, the system frequency response when the BESS is turned off is shown in dotted style in Fig. 8. In the no BESS case, the frequency is over oscillating, its minimum/maximum are greater 0.9899/1.0023 and the steady state is reached later at $t = 7.716$ s. Although it is not shown, the voltage variations in the no BESS case are 0.9748/1.0091, also greater than the ones obtained in the BESS case.

4.2 Positive load step. Peak shaving

At $t = 8.2$ s an extra 100 kW resistive load is connected to the system (33% of the DG rated power), as it can be observed in the load active power curve in Fig. 10. This load step leads the isolated power system to an active power deficit and a system frequency fall. The DG reacts by increasing its generated power and when it is over its 300 kW rated power, the DG overload power protection is activated. This protection increases the power produced by the BESS, so that the DG produced power falls within the 294–300 kW DG maximum power interval. Fig. 10 also presents brief oscillations in the WTG, DG, BESS and load active powers after the positive load step. The variations in the power consumed by the load are due to the voltage variations since the load is purely resistive. The transient finishes at $t = 14.147$ s with WTG producing the 50 kW as the wind speed has not changed, the DG producing 298 kW (a value in the 98–100% $P_{SM\text{-}NOM}$ range) and the BESS producing 77 kW. During this +100 kW load step, the frequency minimum/maximum are 0.9957/1.0012 pu and voltage minimum/maximum are 0.9853/0.9978 pu respectively. In the no BESS case the system frequency falls continuously (dotted line in Fig. 8) as the DG is unable to supply the power needed by the load. Unless another DG is connected quickly to increase the system total rated power, the WDPS heads to a blackout when the minimum system frequency is reached and the corresponding protection trips all the circuit breakers, so that the BESS increases the isolated power system reliability.

The battery variables are shown in Fig. 11 with the same criteria of positive current if the battery is discharging. As in the simulations of WO mode, the battery current also resembles a scaled version of the BESS active power in Fig. 10. The current peak is +0.305 pu (discharging) during the −2 m/s wind step and the steady-state current value is 0 since the DG supplies the needed power. After the +100 kW load step the current in the steady state is +0.5175 pu as the BESS supplies 77 kW. The battery SOC, initially set at 75%, barely changes during the negative wind step due to the short simulation time and its relatively great capacity. After the positive

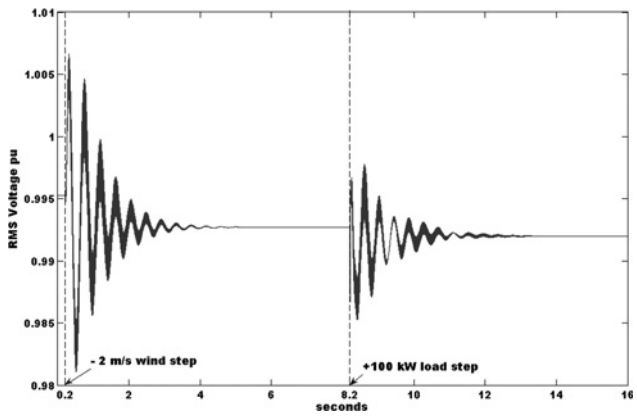

Fig. 9 *WD mode RMS voltage per unit*

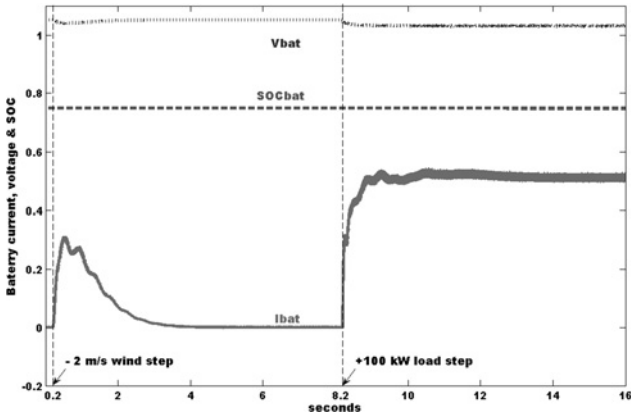

Fig. 11 *WD mode battery current, voltage and SOC*

load step at 8.2 s, SOC decreases continuously but very little being its final value at the end of simulation 74.82%. The voltage variations follow the current variations due to the internal battery resistance since SOC variations are negligible. The lowest voltage is due to the positive peak current after the +100 kW step.

The WD mode simulation has been presented in first place for a negative wind speed step. When compared with the no BESS case, the BESS actuation under the command of the PD regulator eliminates the over shooting in the system frequency, reduces the frequency peaks and voltage variations and shortens the settling time, so that the WDPS power quality is improved in the WD mode.

The positive load step at $t = 8.2$ s would have led the system to a DG overload. It has been shown how the control prevents the DG overload by an integral action that increases the BESS produced power until the DG power falls in a maximum predetermined power interval close to its rated power. The BESS stored power is limited, so the control must order to start and connect another DG in order to stop the BESS from producing power. In a no-storage WDPS the overload simulated case will have led to a blackout, so the BESS assures the power continuity.

5 Conclusions

It has been shown how the BESS under the command of a PID controller regulates the system frequency of the WDPS in the WO mode. The BESS also allows temporarily the WO mode even with the wind power produced lower than the consumed load, so the WDPS reliability is increased. In the WD mode, the BESS improves the system transients and therefore the WDPS power quality. Additionally a peak-shaving simulation is presented where the WD control orders the BESS to supply power temporarily in a DG overload situation improving the power supply continuity and so the WDPS reliability is augmented.

6 References

1 Hunter, R., Elliot, G. (Eds.): 'Wind-diesel systems: a guide to the technology and its implementations' (Cambridge University Press, UK, 1994)

2 Beyer, H.G., Degner, T., Gabler, H.: 'Operational behaviour of wind diesel systems incorporating short-term storage: an analysis via simulation calculations', *Sol. Energy*, 1995, **54**, (6), pp. 429–439

3 Shirazi, M., Droulihet, S.: 'An analysis of the performance benefits of short-term energy storage in wind–diesel power hybrid systems'. 1997 ASME Wind Energy Symp., Reno, Nevada, January 6–9, 1997

4 Suvire, G.O., Mercado, P.E.: 'DSTATCOM with flywheel energy storage system for wind energy applications: control design and simulation', *Electr. Power Syst. Res.*, 2010, **80**, (3), pp. 345–353. ISSN 0378-7796, http://dx.doi.org/10.1016/j.epsr.2009.09.020

5 Abdel-Khalik, A., Elserougi, A., Massoud, A., *et al.*: 'A power control strategy for flywheel doubly-fed induction machine storage system using artificial neural network', *Electr. Power Syst. Res.*, 2013, **96**, pp. 267–276, http://dx.doi.org/10.1016/j.epsr.2012.11.012

6 Muyeen, S.M., Takahashi, R., Murata, T., *et al.*: 'Application of STATCOM/BESS for wind power smoothening and hydrogen generation', *Electr. Power Syst. Res.*, 2009, **79**, (2), pp. 365–373, doi: 10.1016/j.epsr.2008.07.007

7 Zeng, J., Zhang, B., Mao, C., *et al.*: 'Use of battery energy storage system to improve the power quality and stability of wind farms'. Int. Conf. on Power System Technology, 2006 (PowerCon 2006), October 22–26, 2006, pp. 1–6, doi: 10.1109/ICPST.2006.321662

8 Sebastián, R.: 'Reverse power management in a wind diesel system with a battery energy storage', *Int. J. Electr. Power Energy Syst.*, 2013, **44**, (1), pp. 160–167, ISSN 0142-0615, http://dx.doi.org/10.1016/j.ijepes.2012.07.029

9 Sebastián, R., Peña-Alzola, R.: 'Control and simulation of a flywheel energy storage for a wind diesel power system', *Int. J. Electr. Power Energy Syst.*, 2015, **64**, pp. 1049–1056, ISSN 0142-0615, http://dx.doi.org/10.1016/j.ijepes.2014.08.017

10 Tarkeshwar, M., Mukherjee, V.: 'Quasi-oppositional harmony search algorithm and fuzzy logic controller for load frequency stabilisation of an isolated hybrid power system', *IET Gener. Transm. Distrib.*, 2015, **9**, (5), pp. 427–444, doi: 10.1049/iet-gtd.2014.0502

11 Muljadi, E., McKenna, H.E.: 'Power quality issues in a hybrid power system', *IEEE Trans. Ind. Appl.*, 2002, **38**, (3), pp. 803–809

12 Sedaghat, B., Jalilvand, A., Noroozian, R.: 'Design of a multilevel control strategy for integration of stand-alone wind/diesel system', *Int. J. Electr. Power Energy Syst.*, 2012, **35**, (1), pp. 123–137

13 Sebastián, R.: 'Modelling and simulation of a high penetration wind diesel system with battery energy storage', *Int. J. Electr. Power Energy Syst.*, 2011, **33**, (3), pp. 767–774, ISSN 0142-0615, http://dx.doi.org/10.1016/j.ijepes.2010.12.034

14 The MathWorks, Inc.: 'SimDriveLine', Simulink (built upon Matlab) block library online documentation. http://www.mathworks.com/access/helpdesk/help/toolbox/physmod/drive/

15 Yeager, K.E., Willis, J.R.: 'Modelling of emergency diesel generators in an 800 Megawatt nuclear power plant', *IEEE Trans. Energy Convers.*, 1994, **8**, (3), pp. 433–441

16 The MathWorks, Inc.: 'SimPowerSystems', Simulink (built upon Matlab) block library online documentation. http://www.mathworks.com/access/helpdesk/help/toolbox/physmod/powersys/

17 Kothari, D.P., Nagrath, I.J.: 'Modern power system analysis' (Tata McGraw-Hill Education, 2003)

18 Gagnon, R., Saulnier, B., Sybille, G., *et al.*: 'Modelling of a generic high-penetration no-storage wind-diesel system using Matlab/power system blockset'. 2002 Global Windpower Conf., Paris, France, April 2002

19 Knudsen, H., Nielsen, J.N.: 'Introduction to the modeling of wind turbines', in Ackermann, T. (Ed.): 'Wind power in power systems' (Wiley, Chicester, UK, 2005), pp. 525–585

20 Sebastian, R.: 'Simulation of the transition from wind only mode to wind diesel mode in a no-storage Wind Diesel System', *Latin Am. Trans. IEEE (Revista IEEE America Latina)*, 2009, **7**, (5), pp. 539–544, doi: 10.1109/TLA.2009.5361191

21 Sebastián, R., Peña Alzola, R.: 'Simulation of an isolated Wind Diesel System with battery energy storage', *Electr. Power Syst. Res.*, 2011, **81**, (2), pp. 677–686, ISSN 0378-7796, http://dx.doi.org/10.1016/j.epsr.2010.10.033

22 Rezkallah, M., Chandra, A.: 'Wind diesel battery hybrid system with power quality improvement for remote communities'. 2011 IEEE Industry Applications Society Annual Meeting (IAS), October 9–13, 2011, pp. 1–6, doi: 10.1109/IAS.2011.6074303

23 Tremblay, O., Dessaint, L.-A., Dekkiche, A.-I.: 'A generic battery model for the dynamic simulation of hybrid electric vehicles'. IEEE Vehicle Power and Propulsion Conf., VPPC 2007, September 9–12, 2007, pp. 284–289

24 Li, X., Hui, D., Lai, X.: 'Battery energy storage station (BESS)-based smoothing control of photovoltaic (PV) and wind power generation fluctuations', *IEEE Trans. Sustain. Energy*, 2013, **4**, (2), pp. 464–473, doi: 10.1109/TSTE.2013.2247428

25 Sebastián, R.: 'Smooth transition from wind only to wind diesel mode in an autonomous wind diesel system with a battery-based energy storage system', *Renew. Energy*, 2008, **33**, (3), pp. 454–466, ISSN 0960-1481, http://dx.doi.org/10.1016/j.renene.2007.03.007

26 Sebastián, R., Pena-Alzola, R.: 'Effective active power control of a high penetration wind diesel system with a Ni–Cd battery energy storage', *Renew. Energy*, 2010, **35**, (5), pp. 952–965